



Available online at www.sciencedirect.com

SCIENCE @ DIRECT®

C. R. Geoscience 338 (2006) 433–446

COMPTES RENDUS



GEOSCIENCE

<http://france.elsevier.com/direct/CRAS2A/>

Geomaterials (Mineralogy)

Synthesis of green rusts by oxidation of Fe(OH)_2 , their products of oxidation and reduction of ferric oxyhydroxides; $E_{\text{h}}-\text{pH}$ Pourbaix diagrams

Jean-Marie R. Génin ^{a,*}, Christian Ruby ^a, Antoine Géhin ^a, Philippe Refait ^b^a Équipe 'Microbiologie et Physique', laboratoire de chimie physique et microbiologie pour l'environnement, UMR 7564 CNRS-université Henri-Poincaré-Nancy-1, & département "Matériaux et Structures", ESSTIN, 405, rue de Vandoeuvre, 54600 Villers-lès-Nancy, France^b Laboratoire d'étude des matériaux en milieux agressifs (LEMMA), EA 3167, université de La Rochelle, av. Michel-Crépeau, 17042 La Rochelle cedex 01, France

Received 17 October 2005; accepted after revision 10 April 2006

Written on invitation of the Editorial Board

Abstract

$\text{Fe}^{\text{II}}-\text{Fe}^{\text{III}}$ hydroxysalt green rusts (GR), $\{\text{Fe}^{\text{II}}_{2/3}\text{Fe}^{\text{III}}_{1/3}(\text{OH})_2\}^{(1/3)+} \cdot \{[(1/3)/n]\text{A}^{n-} \sim (m/n)\text{H}_2\text{O}\}^{(1/3)-}$, are prepared by oxidising a Fe(OH)_2 precipitate in presence of anions A^{n-} (Cl^- , SO_4^{2-} , CO_3^{2-}). Electrode potential E_{h} and pH recorded during aerial oxidation depend on the initial ratio $R = \{[\text{OH}^-]/[\text{Fe}^{\text{II}}]\}$. For $R = R_{\text{h}} = 2$, i.e. Fe(OH)_2 stoichiometry, two stages are observed and magnetite Fe_3O_4 forms. In contrast, an excess of Fe^{2+} ions, i.e. $R < R_{\text{h}}$, gives rise to 3 stages described in a mass balance diagram: A around pH 7.2 ends at inflection point t_g , B around pH 6.5 at t_f and C around pH 3.5 for strong acids and 9 for buffered solutions. GR forms alone at t_g if initial ratio $R = R_g = 1.67$. Fast oxidation by H_2O_2 , dry oxidation or voltammetry lead to deprotonated GR whereas bioreduction yields deprotonated $\{\text{Fe}^{\text{II}}_{6(1-x)}\text{Fe}^{\text{III}}_{6x}\text{O}_{12}\text{H}_{2(7-3x)}\}^{2+} \cdot [\text{CO}_3^{2-}] \sim 3\text{H}_2\text{O}\}^{2-}$ fougérite with $x \in [1/3, 2/3]$. $E_{\text{h}}-\text{pH}$ diagrams for hydroxycarbonate, chloride, or sulphate are presented. *To cite this article: J.-M.R. Génin et al., C. R. Geoscience 338 (2006).*

© 2006 Académie des sciences. Published by Elsevier SAS. All rights reserved.

Résumé

Synthèse des rouilles vertes par oxydation de Fe(OH)_2 , leurs produits d'oxydation et réduction des oxyhydroxydes ferriques ; diagrammes $E_{\text{h}}-\text{pH}$. Les rouilles vertes, hydroxysels ferreux-ferriques de formule $\{\text{Fe}^{\text{II}}_{2/3}\text{Fe}^{\text{III}}_{1/3}(\text{OH})_2\}^{(1/3)+} \cdot \{[(1/3)/n]\text{A}^{n-} \sim (m/n)\text{H}_2\text{O}\}^{(1/3)-}$ se préparent par oxydation d'un précipité de Fe(OH)_2 en présence d'anions A^{n-} tels que Cl^- , SO_4^{2-} , CO_3^{2-} . Potentiel d'électrode E_{h} et pH enregistrés au cours de l'oxydation à l'air dépendent du rapport initial $R = \{[\text{OH}^-]/[\text{Fe}^{\text{II}}]\}$. À stoichiométrie de Fe(OH)_2 si $R = R_{\text{h}} = 2$, deux étapes s'observent formant Fe_3O_4 . En revanche, l'excès d'ions Fe^{2+} , si $R < R_{\text{h}}$, entraîne trois étapes : A autour de pH 7,2 finit au point d'infexion t_g , B autour de pH 6,5 à t_f et C autour de pH 3,5 pour les acides forts et 9 pour les solutions tamponnées. À t_g , la rouille verte se forme seule, si initialement $R = R_g = 1,67$. Ces étapes s'inscrivent dans un diagramme bilan matière. Oxydation rapide par H_2O_2 , séche ou voltampérométrie conduisent à une rouille verte déprotonée, alors que la bioréduction donne la fougérite $\{\text{Fe}^{\text{II}}_{6(1-x)}\text{Fe}^{\text{III}}_{6x}\text{O}_{12}\text{H}_{2(7-3x)}\}^{2+} \cdot [\text{CO}_3^{2-}] \sim 3\text{H}_2\text{O}\}^{2-}$,

^{*} Corresponding author.E-mail address: genin@lcpme.cnrs-nancy.fr (J.-M.R. Génin).

où $x \in [1/3, 2/3]$. Enfin, sont présentés les diagrammes E_h -pH des rouilles vertes des espèces carbonate, chlorure et sulfate. **Pour citer cet article : J.-M.R. Génin et al., C. R. Geoscience 338 (2006).**

© 2006 Académie des sciences. Published by Elsevier SAS. All rights reserved.

Keywords: Green rusts; Iron oxides; E_h -pH Pourbaix diagrams; Mass-balance diagram

Mots-clés : Rouilles vertes ; Oxydes de fer ; Diagrammes E_h -pH ; Diagramme bilan matière

1. Introduction

$\text{Fe}^{\text{II-III}}$ hydroxysalt green rusts (GR) were long ago recognised as transitory intermediate products during the wet corrosion of iron-base materials. For instance, Girard, entitling his thesis work in 1935 “de la constitution des rouilles” [10], attributed a green compound forming in a sulphated medium to a hydrated magnetite. Thus, the preparation of GRs by oxidation of $\text{Fe}(\text{OH})_2$ was the predilection of corrosion scientists that essentially tried to simulate the process of oxidation of Fe species. It was used extensively for many years in several aqueous solutions containing the major anions Cl^- , SO_4^{2-} , CO_3^{2-} , but also F^- , I^- , Br^- , SO_3^{2-} , $\text{S}_2\text{O}_3^{2-}$, $\text{C}_2\text{O}_4^{2-}$, SeO_4^{2-} [2,5,6,14–18,24,25]. In contrast, NO_3^- , PO_4^{3-} or OH^- , never gave successful results. During aerial exposure of the solution, the electrode potential E_h and pH of the aqueous solution are recorded and the precipitates are filtered and analysed by XRD and Mössbauer spectroscopy. In particular, any salient point in the curves is carefully analysed since it is assumed to correspond to particular conditions in the reaction process. This method for preparing GRs became very reliable but is obviously cumbersome and not so efficient in comparison with the coprecipitation method [3,22,23]. However, the E_h and pH curves gave very valuable thermodynamic information that allowed us to draw the E_h -pH Pourbaix diagrams. These experiments were completed by determining the end products of oxidation, which were very various and were essential for understanding the properties of corroded materials. A comparison with a fast oxidation of GR as done with H_2O_2 or a slow oxidation after drying or by voltammetry or by bacterial reduction of ferric oxyhydroxides is also made in this article for clarity. It is the clue of the formation of partially deprotonated $\text{Fe}^{\text{II-III}}$ hydroxycarbonate fougérite in anoxic gleysols that could be written in its general form $[\text{Fe}^{\text{II}}_{6(1-x)}\text{Fe}^{\text{III}}_{6x}\text{O}_{12}\text{H}_{2(7-3x)}]^{2+} \cdot [\text{CO}_3^{2-} \cdot \sim 3\text{H}_2\text{O}]^{2-}$, where x lies in the $[1/3, 2/3]$ interval.

2. Aerial oxidation of $\text{Fe}(\text{OH})_2$ within solution

2.1. Experimental E_h and pH versus time curves

Ferrous hydroxide precipitated into solution by mixing a ferrous salt comprising anion A^{n-} with caustic soda. In most studies, initial conditions were given by a ratio $\{[\text{Fe}^{2+}]/[\text{OH}^-]\} = \{[\text{FeA}_{(2/n)}]/[\text{NaOH}]\}$ of the concentration of ferrous salt over that of NaOH most often comprised between 0.2 and 0.4 mol l⁻¹. It is equivalent to R^{-1} as named in the coprecipitation method where R was defined as $\{[\text{OH}^{-1}]/[\text{Fe}_{\text{total}}]\}$ [3,22,23]. Then, the solution was stirred in the presence of air at constant velocity in a beaker with a magnetic rod and two electrodes recorded pH and potential using a calomel electrode as a reference, even though the potential E_h was reported with respect to the standard hydrogen electrode (SHE). Ferrous chloride $\text{FeCl}_2 \cdot 4\text{H}_2\text{O}$ and melanterite $\text{FeSO}_4 \cdot 7\text{H}_2\text{O}$ were appropriate for Cl^- and SO_4^{2-} , but it became much less easier for CO_3^{2-} anions, since carbonate salts were not soluble; $\text{Fe}(\text{OH})_2$ precipitated with ferrous sulphate before adding sodium carbonate to obtain $\text{GR1}(\text{CO}_3^{2-})$ [5]. The same was done for $\text{GR1}(\text{SO}_3^{2-})$ [24], $\text{GR2}(\text{S}_2\text{O}_3^{2-})$ [17], and $\text{GR2}(\text{SeO}_4^{2-})$ [18]. In presence of an excess of ferrous salt to precipitate $\text{Fe}(\text{OH})_2$, typical curves of E_h and pH vs. time curves display three stages (Fig. 1). A first one (A) ends at the inflection point t_g where all ferrous hydroxide is transformed into GR incorporating present anions A^{n-} . During a second stage B ending at inflection point t_f , the GR oxidises into the usual ferric rusts and disappears completely. A third stage C from t_f to t_∞ corresponds to the oxidation of Fe^{II} ions left within the solution. Fig. 1 reports specifically the case of the sulphate medium, which is chosen here since it was the most widely studied system, setting the initial concentrations at $R = R_g = (5/3) = 1.67$ to obtain solely $\text{GR2}(\text{SO}_4^{2-})$ [6]. Samples of transient compounds during oxidation were analysed by Mössbauer spectroscopy at 15 K (Fig. 2) where they were set in a holder inside the cryostat only a few seconds after filtration.

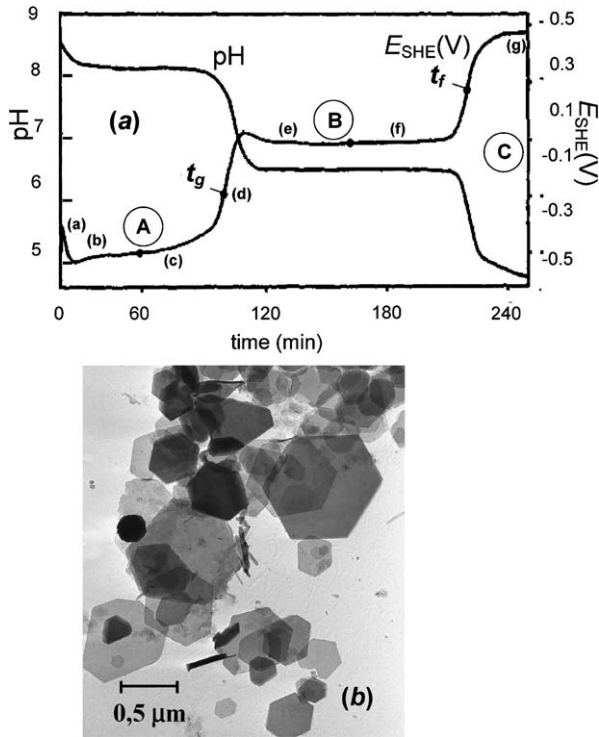


Fig. 1. (a) Zero-current potential E_h (SHE) and pH vs. time curves recorded during the oxidation of an aerated suspension of ferrous hydroxide in a sulphate containing medium for initial ratio $R = \{[\text{OH}^-]/[\text{Fe}_{\text{total}}]\} = R_g = 1.67$. Three stages A, B and C illustrated by plateaus when E_h and pH stay constant correspond to three equilibrium reactions. At t_g , 100% of $\text{GR}_2(\text{SO}_4^{2-})$ forms and at t_f there exist only one solid phase, lepidocrocite $\gamma\text{-FeOOH}$ with Fe^{II} ions within solution. Points (a)–(g) indicate the times at which the precipitates analysed by Mössbauer spectroscopy were sampled [6]. (b) Transmission electron micrograph of sample of GR at t_g [6].

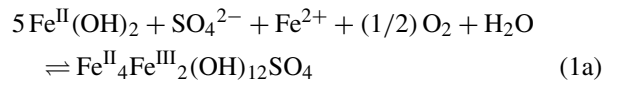
Fig. 1. (a) Courbes du potentiel d'électrode à courant nul E_h (SHE) et pH, enregistrées en fonction du temps au cours de l'oxydation à l'air d'une suspension d'hydroxyde ferreux dans un milieu contenant du sulfate pour un rapport initial $R = \{[\text{OH}^-]/[\text{Fe}_{\text{total}}]\} = R_g = 1.67$. Trois étapes A, B et C, illustrées par des plateaux où E_h et pH restent constants, correspondent à trois réactions à l'équilibre. À t_g , 100% de rouille verte se forme et à t_f existe une seule phase solide, la lépidocrocite $\gamma\text{-FeOOH}$, en compagnie d'ions Fe^{II} en solution. Les points (a)–(g) indiquent les moments où ont été prélevés les échantillons en vue de l'analyse par spectrométrie Mössbauer [6]. (b) Micrographie électronique en transmission d'échantillon de rouille verte prélevé à t_g [6].

2.2. Mass-balance diagram

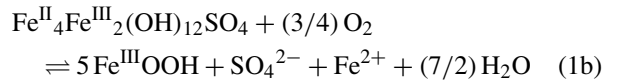
2.2.1. Formation of green rust ($R_g = 1.67$)

Interpretation of the E_h and pH versus time curves is easy within the frame of the mass-balance diagram where $R = \{[\text{OH}^-]/[\text{Fe}_{\text{total}}]\}$ is plotted versus $x = \{[\text{Fe}^{\text{III}}]/[\text{Fe}_{\text{total}}]\}$ (Fig. 3) [22,23]. Initial conditions are shown in the diagram by a point on the co-ordinate axis

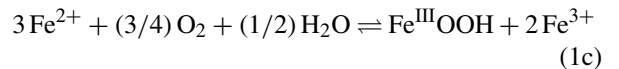
that corresponds to a mixture of the initial precipitate of $\text{Fe}(\text{OH})_2$ at point G, $(R, x) = (0, 2)$, and Fe^{II} within solution at F, $(0, 0)$. During the overall oxidation process, $\text{Fe}(\text{OH})_2$ transforms into FeOOH and reaction paths follow straight lines with a slope of 1 (Fig. 3). Therefore, the straight line that goes directly through the point representing $\text{GR}_2(\text{SO}_4^{2-})$ at $(0.33, 2)$ has for co-ordinate at origin $(0, 1.67)$; $R_g = (5/3) = 1.67$ is the initial value of R to obtain 100% of GR with an excess of Fe^{II} with respect to $\text{Fe}(\text{OH})_2$ at $R = R_h = 2$. Stage A that starts at point A (t_{0g}) to end at B (t_g) is thus the oxidation of $\text{Fe}(\text{OH})_2$ (cf. Fig. 2a) into $\text{GR}_2(\text{SO}_4^{2-})$ (cf. Fig. 2d) using this initial excess of Fe^{II} and anions at $R = R_g$:



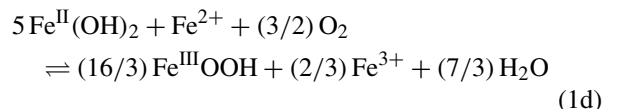
Then, stage B that elapses from point B (t_g) to C (t_f) is the oxidation of $\text{GR}_2(\text{SO}_4^{2-})$ into FeOOH , here lepidocrocite, that releases Fe^{2+} ions and anions into solution:



Then, during stage C, Fe^{2+} within solution gets oxidised into FeOOH (cf. Fig. 2g) for one third of it and 2/3 in solution; the solution gets acidic gradually (cf. Fig. 1a):



As a whole, the initial $\text{Fe}(\text{OH})_2$ at point A becomes ferric oxyhydroxide $\alpha\text{-FeOOH}$ goethite and Fe^{3+} ions in acidic solution at point D according to:



At D on tie-line EI, the mixture of FeOOH and Fe^{3+} is in the 8:1 proportion (Eq. (1d)).

2.2.2. Formation of magnetite ($R_h = 2$)

The direct oxidation of $\text{Fe}(\text{OH})_2$ at stoichiometry, i.e. initially at $R = R_h = 2$, that starts at t_{0m} (point G) corresponds to the 2 reactions D and E where the E_h and pH vs. time curves present only one inflection t_m (point H) (Fig. 3). $\text{Fe}(\text{OH})_2$ becomes directly magnetite Fe_3O_4 and then magnetite gradually transforms in situ into $\gamma\text{-Fe}_2\text{O}_3$ maghemite (point E) rather than into FeOOH , since maghemite has the same spinel structure. Reactions are respectively:



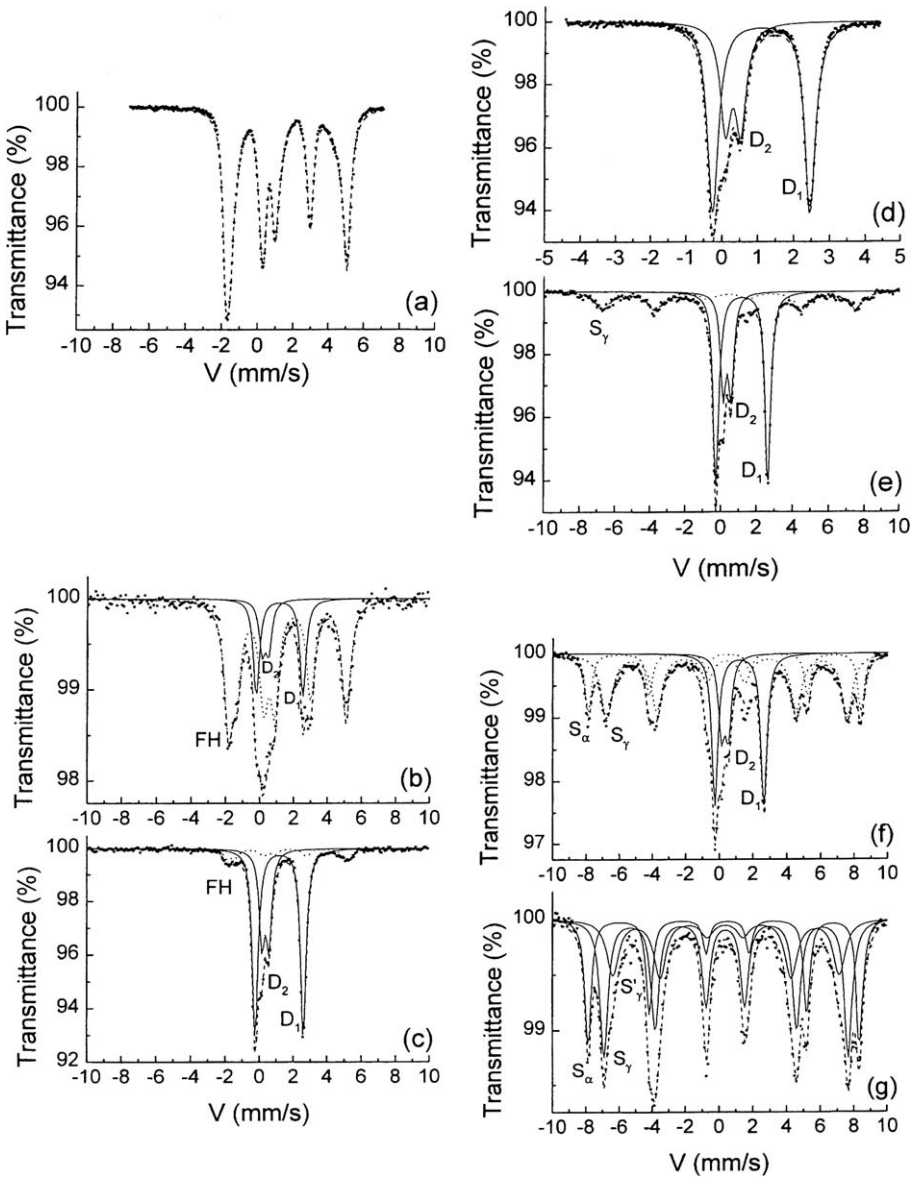
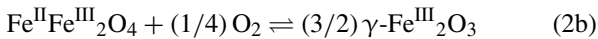


Fig. 2. Transmission Mössbauer spectra measured at 15 K of the solid phases sampled at various times of the oxidation of ferrous hydroxide. Times (a)–(g) of sampling are indicated on the E_h vs. time curve of Fig. 1 [6]. (a) Ferrous hydroxide prepared in basic medium, (b) and (c) in plateau A during the first stage: a mixture of ferrous hydroxide and GR, (d) at t_g , GR is alone, (e) and (f) during the second stage in plateau B, γ -FeOOH and then α -FeOOH increase at the expense of GR, (g) during the last plateau C, there are only α - and γ -FeOOH as solid phases.

Fig. 2. Spectres Mössbauer par transmission mesurés à 15 K des phases solides prélevées à diverses périodes de l'oxydation de l'hydroxyde ferreux [6]. Les instants de prélèvement de (a) à (g) sont indiqués sur la courbe E_h en fonction du temps de la Fig. 1. (a) Hydroxyde ferreux préparé en milieu basique, (b) et (c) mélange d'hydroxyde ferreux et de rouille verte sur le plateau A au cours de la première étape, (d) la rouille verte est seule à t_g , (e) et (f) au cours de la seconde étape sur le plateau B, γ -FeOOH, puis α -FeOOH croissent au dépens de la rouille verte, (g) au cours du dernier plateau C ne se trouvent que les phases solides α - et γ -FeOOH.



It is clear that no route exists to go merely from a GR to magnetite by aerial oxidation within solution. It has been claimed sometimes in corrosion science that a GR should be the precursor of magnetite [13]. If this would occur it could not be simply by aerial oxidation.

2.2.3. Trigger value $R_c = 1.714$

It has been carefully established by coprecipitation of Fe^{II} and Fe^{III} ions in the presence of SO_4^{2-} that the formation of $\text{GR}_2(\text{SO}_4^{2-})$ necessitates an excess of OH^- ions [22,23]. This surprising result at a first glance comes from the mechanism of formation of the

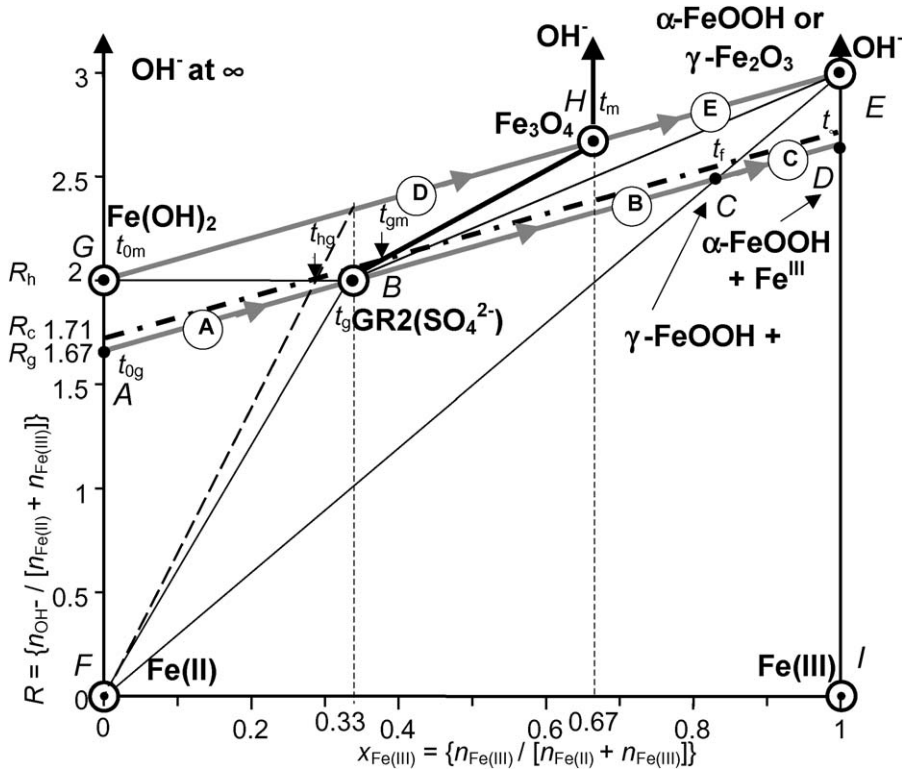


Fig. 3. Mass-balance diagram of iron species in a sulphate containing medium where $\text{GR2}(\text{SO}_4^{2-})$ forms. Three routes are drawn to illustrate the aerial oxidation of Fe(OH)_2 where initial values of R are $R_h = 2$, $R_c = 1.714$ and $R_g = 1.67$.

Fig. 3. Diagramme bilan matière des espèces du fer dans un milieu contenant des ions sulfate où se forme $\text{GR2}(\text{SO}_4^{2-})$. Trois cheminement sont représentés pour illustrer l'oxydation à l'air de Fe(OH)_2 où les valeurs initiales de R sont $R_h = 2$, $R_c = 1,714$ et $R_g = 1,67$.

GR where Fe(OH)_2 layers grow parallel to the surface of the solid ferric oxyhydroxide by trapping anions in between and electron transfer takes place from Fe^{II} to the ferric substrate [23]. The $\text{GR2}(\text{SO}_4^{2-})$ particle grows progressively and will separate from the shrinking FeOOH crystal sooner or later. Line $R = 7 \times x$ thus plays a specific role and its intersect with $R = 2$ separates two different behaviours corresponding to a value $R = R_c = (12/7) = 1.714$ (Fig. 3). When $R_h = 2 > R > R_c = 1.714$, the straight line cuts tie-line GB joining Fe(OH)_2 and $\text{GR2}(\text{SO}_4^{2-})$ before that joining $\text{GR2}(\text{SO}_4^{2-})$ and Fe_3O_4 , i.e. BH. This mixture evolves into FeOOH and some magnetite may remain. If $R_c = 1.714 > R > R_g = 1.67$, all Fe(OH)_2 transforms into $\text{GR2}(\text{SO}_4^{2-})$ and no magnetite is observed.

2.3. Products of oxidation within solution

2.3.1. Lepidocrocite and goethite for $\text{GR1}(\text{Cl}^-)$ and $\text{GR2}(\text{SO}_4^{2-})$ in acidic medium

The determination of the products of oxidation of GRs are of major importance for some technological

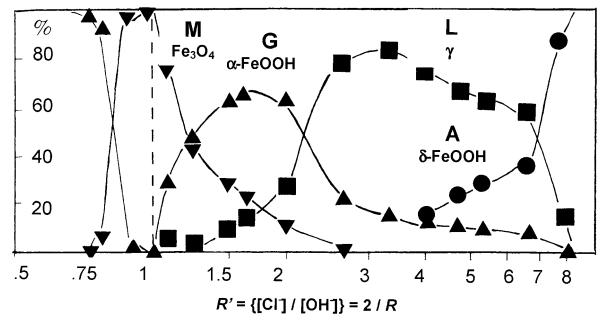


Fig. 4. End-products of the aerial oxidation of Fe(OH)_2 in chloride containing medium with respect to the initial ratio $R' = \{[\text{Cl}^-]/[\text{OH}^-]\} = 2/R$ [13,14]. ▼ M: Magnetite, ▲ G: goethite, ■ L: lepidocrocite, ● A: akaganeite.

Fig. 4. Produits finals de l'oxydation à l'air de Fe(OH)_2 en milieu chloruré en fonction du rapport initial $R' = \{[\text{Cl}^-]/[\text{OH}^-]\} = 2/R$ [13,14]. ▼ M : Magnétite, ▲ G : goéthite, ■ L : lépidocrocite, ● A : akaganéite.

issues involving corrosion and environmental science as well. It is also a topic by itself for explaining the genesis of minerals. Early works were devoted to the final products of oxidation of Fe(OH)_2 when vary-

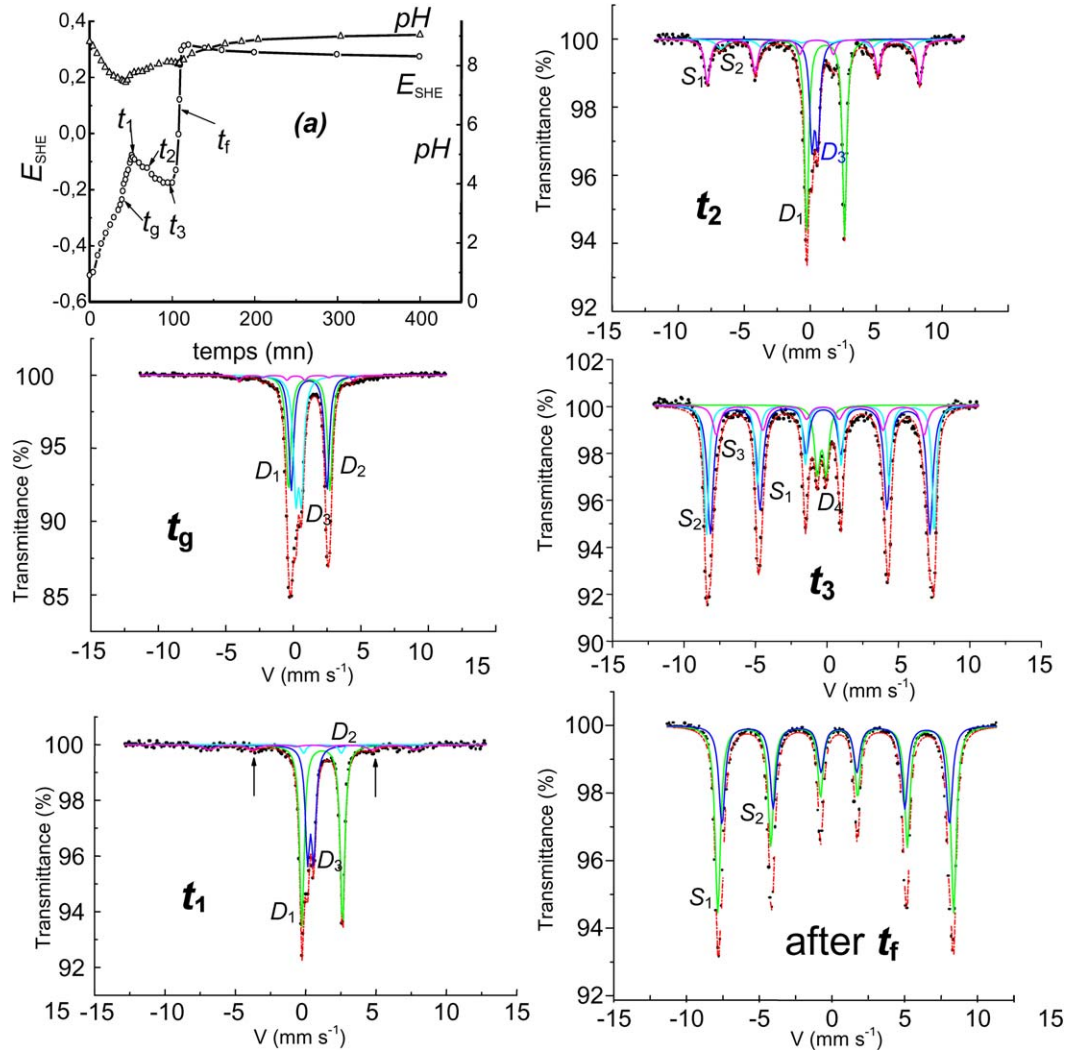


Fig. 5. Aerial oxidation of $\text{Fe}(\text{OH})_2$ in the carbonate-containing solution and corresponding Mössbauer spectra showing the formation of ferrihydrite at the end of stage B before transforming into goethite. The solution is buffered by HCO_3^- ions around pH 9. D_1, D_2, D_3 : GR1(CO_3^{2-}) doublets, S_1 : ferrihydrite sextet, S_2, S_3 : goethite sextets, D_4 : ferrihydrite doublet, t_g : some GR1(CO_3^{2-}) alone, t_1 : GR1(CO_3^{2-}) + some ferrihydrite, t_2 : GR1(CO_3^{2-}) + goethite + ferrihydrite, t_3 : goethite + ferrihydrite. After t_f : goethite alone.

Fig. 5. Oxydation à l'air de $\text{Fe}(\text{OH})_2$ en solution carbonatée et spectres Mössbauer afférents montrant la formation de ferrihydrite en fin d'étape B, avant transformation en goethite. La solution est tamponnée par les ions HCO_3^- aux alentours de pH 9.

ing the initial ratio $R = \{[\text{OH}^-]/[\text{Fe}_{\text{total}}]\}$. This is illustrated for the chloride-containing medium where $R' = \{\text{Cl}^-\}/[\text{OH}^-] = 2R^{-1}$ [16]. Mössbauer spectroscopy was used for analysing the final products (Fig. 4). Magnetite is obtained for $R' \sim 1$, i.e. $R \sim 2$, then goethite $\alpha\text{-FeOOH}$ is maximum for $R' \sim 1.67$. Then lepidocrocite $\gamma\text{-FeOOH}$ is overwhelming around $R' = 3.5$, whereas akaganeite $\beta\text{-FeOOH}$ begins to appear for $R' = 4$ and is alone for $R' = 8$. A comparable result is observed for the sulphate containing medium, i.e. magnetite for $R \sim 2$, then an increase of goethite that drops suddenly at $R = R_c = 1.714$ where lepi-

docracite appears at 75% and decreases slowly along with a new increase of goethite. In both examples, lepidocrocite appears at the end of stage B before it transforms into $\alpha\text{-FeOOH}$ according to reaction (1c) in acidic conditions if GRs form as its precursor in the pathway.

2.3.2. Ferrihydrite and goethite for GR1(CO_3^{2-}) in basic medium

The carbonate-containing medium behaves differently at $R_g = 5/3$; GR1(CO_3^{2-}) transforms into ferrihydrite, which itself transforms into goethite later on

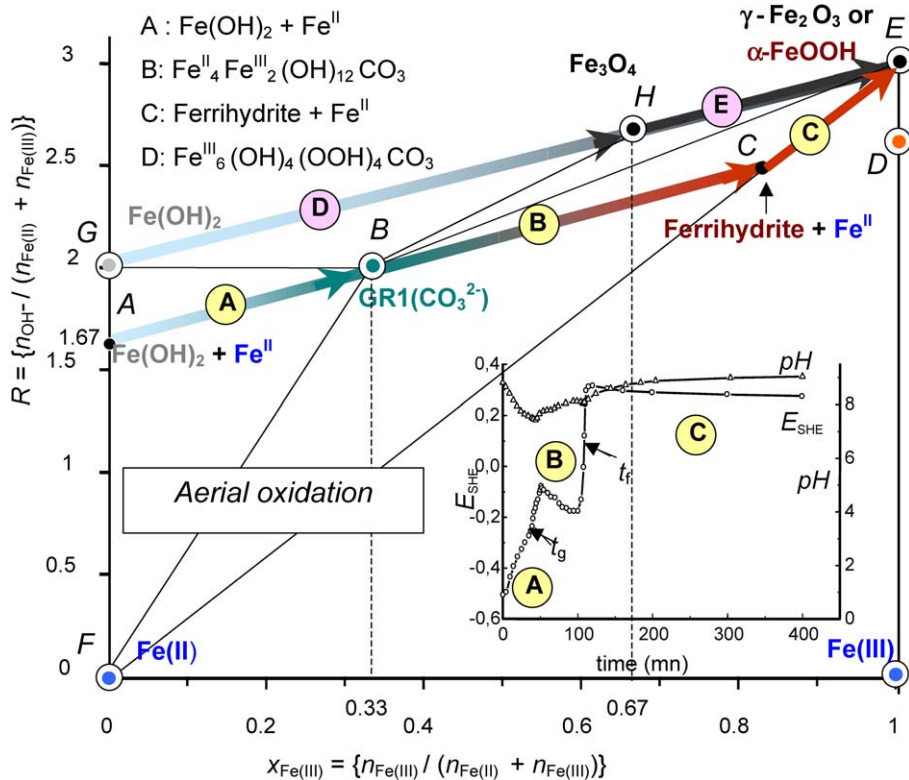


Fig. 6. Mass-balance diagram comprising $\text{Fe}^{\text{II}}\text{--}\text{III}$ hydroxycarbonate green rust GR1(CO_3^{2-}) at stoichiometry, i.e. $x = 1/3$. The path followed during the aerial oxidation of $\text{Fe}(\text{OH})_2$ with an excess of $\text{Fe}^{2+}_{\text{aq}}$ is stressed displaying the three stages, AB, BC, CE, as observed in E_h or pH vs. time curves (inset). The final ferric oxyhydroxide is ferrihydrite at point C (stage B) that transforms slowly into goethite (stage C) from C to E.

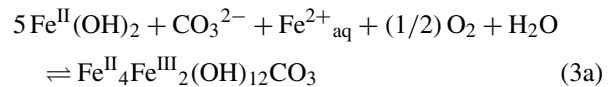
Fig. 6. Diagramme bilan matière comportant l'hydroxycarbonate ferreux-ferrique GR1(CO_3^{2-}) rouille verte à la stéchiométrie, c'est-à-dire $x = 1/3$. Le chemin suivi au cours de l'oxydation à l'air de $\text{Fe}(\text{OH})_2$ en excès de $\text{Fe}^{2+}_{\text{aq}}$ est souligné, montrant les trois étapes, AB, BC, CE, observées sur les courbes E_h ou pH en fonction du temps (encart). L'oxyhydroxyde ferrique final est la ferrihydrite au point C (étape B), qui se transforme lentement en goethite (étape C) de C à E.

(Fig. 5) [1]. It was demonstrated that the evolution could be stopped by the adsorption of anions such as phosphate onto ferrihydrite. Field observations that ferrihydrite of reddish brown colour forms in waterlogged soils where bluish green fougereite lies are a good indication that the hydroxycarbonate is indeed concerned.

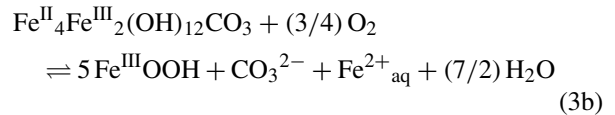
Fig. 6 allows comparing the reaction path in the case of the carbonated medium with those of chloride and sulphate media. The two first stages are similar and correspond to the same reactions: stage A is the oxidation of $\text{Fe}(\text{OH})_2$ into the GR at t_g incorporating the afferent anion and stage B the oxidation of GR giving FeOOH (ferrihydrite or lepidocrocite) by releasing Fe^{II} ions and intercalated anions into solution at t_f . However, stage C is quite different, since the solution is now buffered by the released HCO_3^- ions; CO_3^{2-} ions within the solid GR become HCO_3^- ions by consuming protons of the solution and thus the pH increases. This is illustrated by the pH curve that remains basic around 9 (inset of

Fig. 6). Consequently, Fe^{II} ions can only get oxidised into Fe^{III} ions that immediately precipitate and the path is line CE that reaches 100% of α -goethite. Finally the three stage reactions become:

Stage A: $\text{Fe}(\text{OH})_2$ gets oxidised by incorporating carbonate ions:

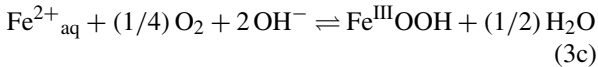


Stage B: GR1(CO_3^{2-}) gets oxidised into ferrihydrite releasing $\text{Fe}^{2+}_{\text{aq}}$ and CO_3^{2-} ions:

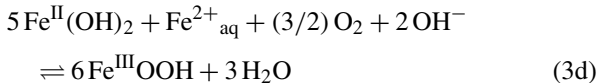


Stage C: $\text{Fe}^{\text{II}}_{\text{aq}}$ gets oxidised participating to the transformation of ferrihydrite into goethite by consum-

ing OH^- ions:



As a whole, Fe(OH)_2 gets oxidised into $\alpha\text{-FeOOH}$ with oxygen by incorporating the excess of $\text{Fe}^{2+}_{\text{aq}}$ from solution along with some OH^- ions in stage C:



Note that for strong acids, e.g., for Cl^- or SO_4^{2-} , stage B yields lepidocrocite and Fe^{II} ions partially oxidising into Fe^{III} within acidic solution (Fig. 1), whereas for buffering carbonate, ferrihydrite forms since Fe^{II} ions cannot become Fe^{III} within a solution that remains basic. Formations of lepidocrocite or ferrihydrite are consequences of the pH of the ending solution.

3. Deprotonation of green rusts

3.1. Fast or dry oxidation

The fast oxidation of GRs by hydrogen peroxide or an aerial oxidation of previously dried GRs gives rise to the fully deprotonated ‘ferric GR’. For instance, in the case of $\text{GR1}(\text{Cl}^-)$, instead of getting the XRD pattern of lepidocrocite or ferrihydrite as for the aerial oxidation in solution, the oxidised product has a pattern quite similar to that initially observed and only lattice parameters are slightly different with blurred and broadened lines [19]; however, its Mössbauer spectrum displays only ferric sextets at 12 K and no ferrous quadrupole doublet at 78 K. Thus, its formula is $[\text{Fe}^{\text{III}}_4\text{O}_8\text{H}_5]^+ \cdot [\text{Cl}^- \sim 2\text{H}_2\text{O}]^{2-}$. Moreover, the compound has a bright orange colour [19]. In the case of $\text{GR1}(\text{CO}_3^{2-})$, we obtain also a ‘ferric $\text{GR1}(\text{CO}_3^{2-})^*$ ’, $[\text{Fe}^{\text{III}}_6\text{O}_{12}\text{H}_8]^{2-} \cdot [\text{CO}_3^{2-} \sim 3\text{H}_2\text{O}]^{2-}$. How to represent

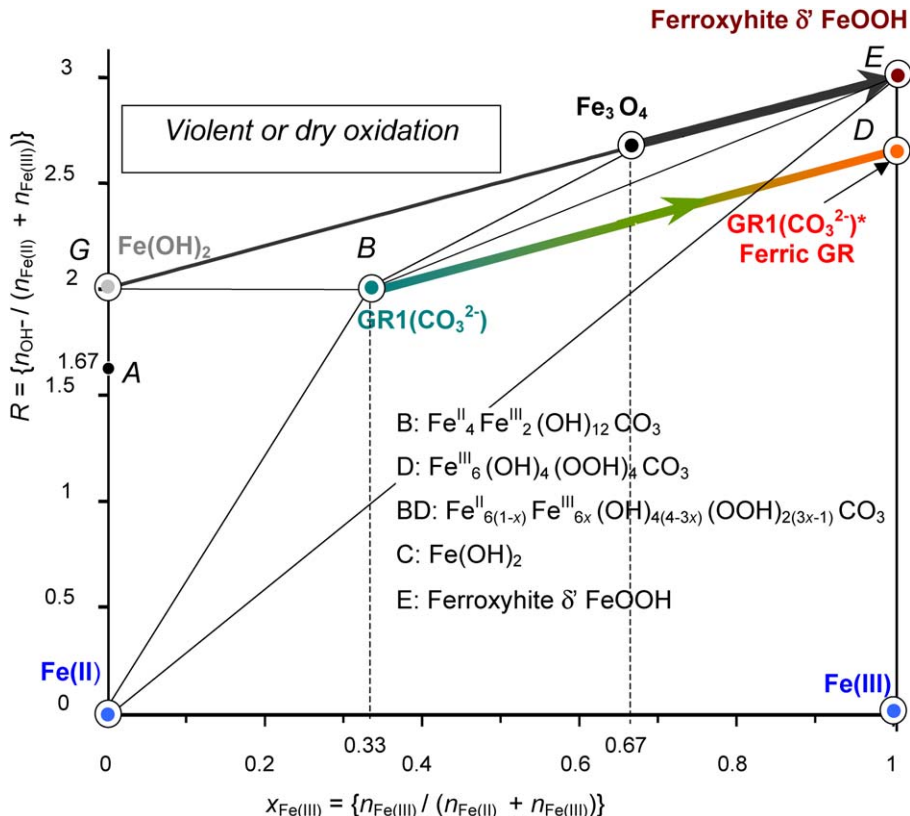
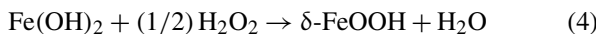


Fig. 7. Mass-balance diagram comprising $\text{Fe}^{\text{II-III}}$ hydroxycarbonate green rust $\text{GR1}(\text{CO}_3^{2-})$ at stoichiometry, i.e. $x = 1/3$ (point B) and ferric $\text{GR1}(\text{CO}_3^{2-})^*$ (point D). The path followed during the fast oxidation of $\text{GR1}(\text{CO}_3^{2-})$ by H_2O_2 is stressed. The final ferric oxyhydroxide is the fully deprotonated green rust $\text{GR1}(\text{CO}_3^{2-})^*$. A similar deprotonation process may occur with Fe(OH)_2 to form $\delta\text{-FeOOH}$ -feroxyhyte mineral.

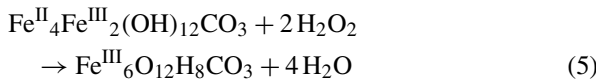
Fig. 7. Diagramme bilan matière comportant l’hydroxycarbonate ferreux-ferrique $\text{GR1}(\text{CO}_3^{2-})$ rouille verte à la stoechiométrie, c'est-à-dire $x = 1/3$ (point B) et sa forme ferrique $\text{GR1}(\text{CO}_3^{2-})^*$ (point D). Le chemin suivi au cours d’une oxydation rapide de $\text{GR1}(\text{CO}_3^{2-})$ par H_2O_2 est souligné. L’oxyhydroxyde ferrique final est la « rouille verte » complètement déprotonée, de couleur orange, $\text{GR1}(\text{CO}_3^{2-})^*$. Un processus similaire de déprotonation peut survenir avec Fe(OH)_2 pour former le minéral feroxyhyte $\delta\text{-FeOOH}$.

this compound in the mass-balance diagram? The initial GR1(CO_3^{2-}) was represented by point B [1/3, 2] and GR1(CO_3^{2-})* by point D [1, 8/3] (Fig. 7). The oxidation path is consequently line BD of slope 1 that joins these two points. A partial deprotonation of GR can be obtained by adjusting precisely the amount of H_2O_2 to aim at an intermediate value of x in the way between 1/3 and 1. Mössbauer spectra have been shown and any point in line BD (Fig. 7) represents such a GR of formula $\text{Fe}^{\text{II}}_{6(1-x)}\text{Fe}^{\text{III}}_{6x}\text{O}_{12}\text{H}_{2(7-3x)}\text{CO}_3$ [9].

The same type of phenomenon occurs if oxidising violently $\text{Fe}(\text{OH})_2$ with H_2O_2 . A phase named δ - FeOOH forms. Its mineral counterpart is feroxyhyte [4]. In both cases, the original crystal lattice is conserved; each $\text{Fe}^{\text{II}}(\text{OH})_6$ octahedron becomes a $\text{Fe}^{\text{III}}(\text{OOH})_3$ octahedron while the Fe^{II} gets oxidised. Reactions are quite similar as shown in the mass-balance diagram (Fig. 7). Starting at point G [0, 2], $\text{Fe}(\text{OH})_2$ for ferrous hydroxide, one ends at point E [1, 3], δ - FeOOH for feroxyhyte, by consuming some OH^- and following path GE according to:



For its part, the fast oxidation of GR1(CO_3^{2-}) that starts at B [1/3, 2] and ends at D [1, 8/3] with also a consumption of OH^- follows accordingly path BD:



3.2. Voltammetry

Voltammetric curves have been drawn to form GR1(CO_3^{2-}) and obtain electrode potential data by using an iron foil [11]. The curve is reversible and a hysteresis occurs in situ during oxidation and reduction (Fig. 8a). SEM picture displays hexagonal orange ferric GR1(CO_3^{2-})* crystals (Fig. 8b); a continuum $\{\text{Fe}^{\text{II}}_{6(1-x)}\text{Fe}^{\text{III}}_{6x}\text{O}_{12}\text{H}_{2(7-3x)}\}^{2+} \cdot [\text{CO}_3^{2-} \sim 3\text{H}_2\text{O}]^{2-}$ exists where x lies all over the [1/3, 1] interval. Using voltammetric curves is common in corrosion science giving valuable information. In this extremely important case – since it deals with the corrosion of iron-made materials and steels –, products and processes can be quite different, due to the various conditions of oxidation that can be encountered. This renders any prediction more difficult.

4. Reduction of FeOOH

The mass-balance diagram was very useful for illustrating the three reaction stages that evolve during the

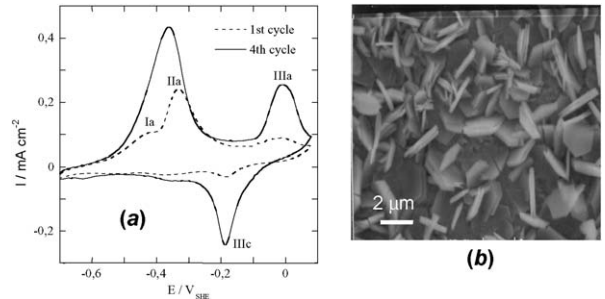


Fig. 8. (a) Voltammograms obtained on iron disc at 10 mV s⁻¹ in 0.4 M NaHCO₃ solution at 25 °C and pH = 9.6. (b) SEM image of the orange ferric compound resulting from the oxidation by air of electrochemically formed GR2(CO_3^{2-}) after ageing at 30 °C for 50 days.

Fig. 8. (a) Voltampérogrammes obtenus avec un disque de fer à 10 mV s⁻¹ dans une solution 0,4 M NaHCO₃ à 25 °C et pH = 9,6. (b) Image au microscope à balayage du composé ferrique orange résultant de l'oxydation à l'air de GR2(CO_3^{2-}) formée électrochimiquement après vieillissement de 50 jours à 30 °C.

oxidation processes of $\text{Fe}(\text{OH})_2$ as discussed previously for aerial oxidation, i.e. by following initially (stages A and B) a straight line of slope 1 (Figs. 3 and 6). Similarly, a fast oxidation as accomplished by using H_2O_2 gave rise to a deprotonation of GR, the ‘ferric GR*’, and the pathway followed also a line of slope 1 from B to D as drawn for the carbonated medium (Fig. 7). How to materialise the pathways when starting from the ferric oxyhydroxides? From point E (1, 3) that represents FeOOH , there are three possibilities (Fig. 9): (i) the dissolution of Fe^{III} in an acidic medium illustrated by a vertical line EI, $x = 1$, that is the tie-line between solid FeOOH and Fe^{3+} ions, (ii) a reductive dissolution following line EF of slope 3 that represents a mixture of FeOOH and Fe^{2+} ions in solution, (iii) a reduction of the solid phase following line EH of slope 1 that reaches Fe_3O_4 .

4.1. Bioreduction of ferric oxyhydroxides

The second pathway EF is followed during the dissimilatory reduction of FeOOH by bacteria (Fig. 9) [12]. The practical role of DIRB is to reduce ferric species from solid state into Fe^{2+} ions that are dissolved in circumneutral medium by enzymatic activity [20,21]. This produces a mixture of Fe^{2+} and FeOOH and the running point migrates from E to F (Fig. 9).

The precipitate that forms depends on the position at which the mixture of FeOOH and Fe^{II} is located before a coprecipitation occurs in relation with the pH of the solution through the value of R . From E to C* where $x = 2/3$, only off-stoichiometric magnetite may

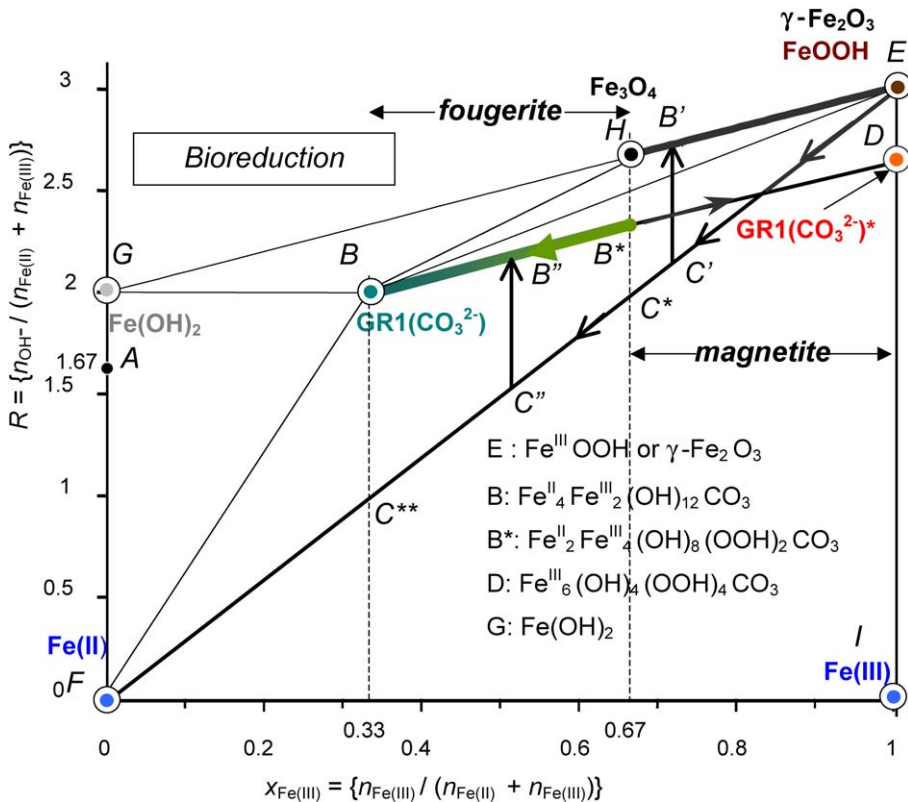
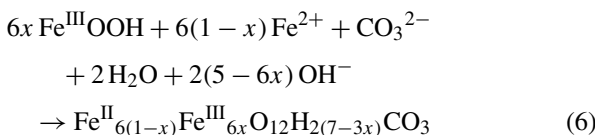


Fig. 9. Mass-balance diagram including Fe^{II}-III hydroxycarbonate green rust GR1(CO₃²⁻) at stoichiometry, i.e. $x = 1/3$ and ferric GR1(CO₃²⁻)*. The paths followed during the bacterial reduction of any ferric oxyhydroxide by dissimilatory iron reducing bacteria (DIRB) are stressed demonstrating that magnetite or partially deprotonated hydroxycarbonate may form depending on the bacterial activity. Fougerite is GR1(CO₃²⁻)* in the range $(1/3) \leq x \leq (2/3)$, whereas magnetite is in the range $(2/3) \leq x \leq 1$.

Fig. 9. Diagramme bilan matière de l'hydroxycarbonate ferreux-ferrique GR1(CO₃²⁻) rouille verte à la stoechiométrie, c'est-à-dire $x = 1/3$ et GR1(CO₃²⁻)* ferrique. Les cheminement suivis au cours de la réduction bactérienne d'un quelconque oxyhydroxyde ferrique par les bactéries ferriréductrices dissimilatives sont soulignés, montrant que la magnétite ou l'hydroxycarbonate partiellement déprotoné peut se former selon l'activité bactérienne. La fougérite se trouve dans le domaine $(1/3) \leq x \leq (2/3)$, alors que la magnétite se trouve dans le domaine $(2/3) \leq x \leq 1$.

form following line C' to B' (Fig. 9). From C* to C**, only GR1(CO₃²⁻)* forms by coprecipitation (C''B'') in circumneutral conditions. The domain of biogenerated hydroxycarbonate corresponds to [1/3, 2/3] and the reaction is:



4.2. The Fe^{II}-III hydroxycarbonate fougerite

Occurrences of GRs in the Gr horizon of a gley soil are consistent with the previous scheme. The mineral is formed by bacterial reduction of ferric oxyhydroxides [8]. Carbonate and Fe^{II} ions come from

the consumption and decomposition of humic substances, and the respiration of bacteria. Route EC''B'' of Fig. 9 is followed, giving rise to partially deprotonated GR1(CO₃²⁻)* where x belongs to the [1/3, 2/3] interval. All fougerite minerals identified up today display Mössbauer spectra where x belongs to this interval.

Therefore, fougerite is $[\text{Fe}^{\text{II}}_{6(1-x)}\text{Fe}^{\text{III}}_{6x}\text{O}_{12}]^{2+} \cdot [\text{CO}_3^{2-} \cdot \sim 3\text{H}_2\text{O}]^{2-}$ where $x \in [1/3, 2/3]$. Some minor substitution of Fe^{II} and Fe^{III} by Mg^{II} and Al^{III} in Nature cannot be excluded.

5. E_h -pH Pourbaix diagrams of green rusts

Monitored aerial oxidation of Fe(OH)₂ was extensively utilised for preparing GRs, but also for determining their composition [5,6,14,17]. The preparation by coprecipitation of Fe^{II} and Fe^{III} species has now

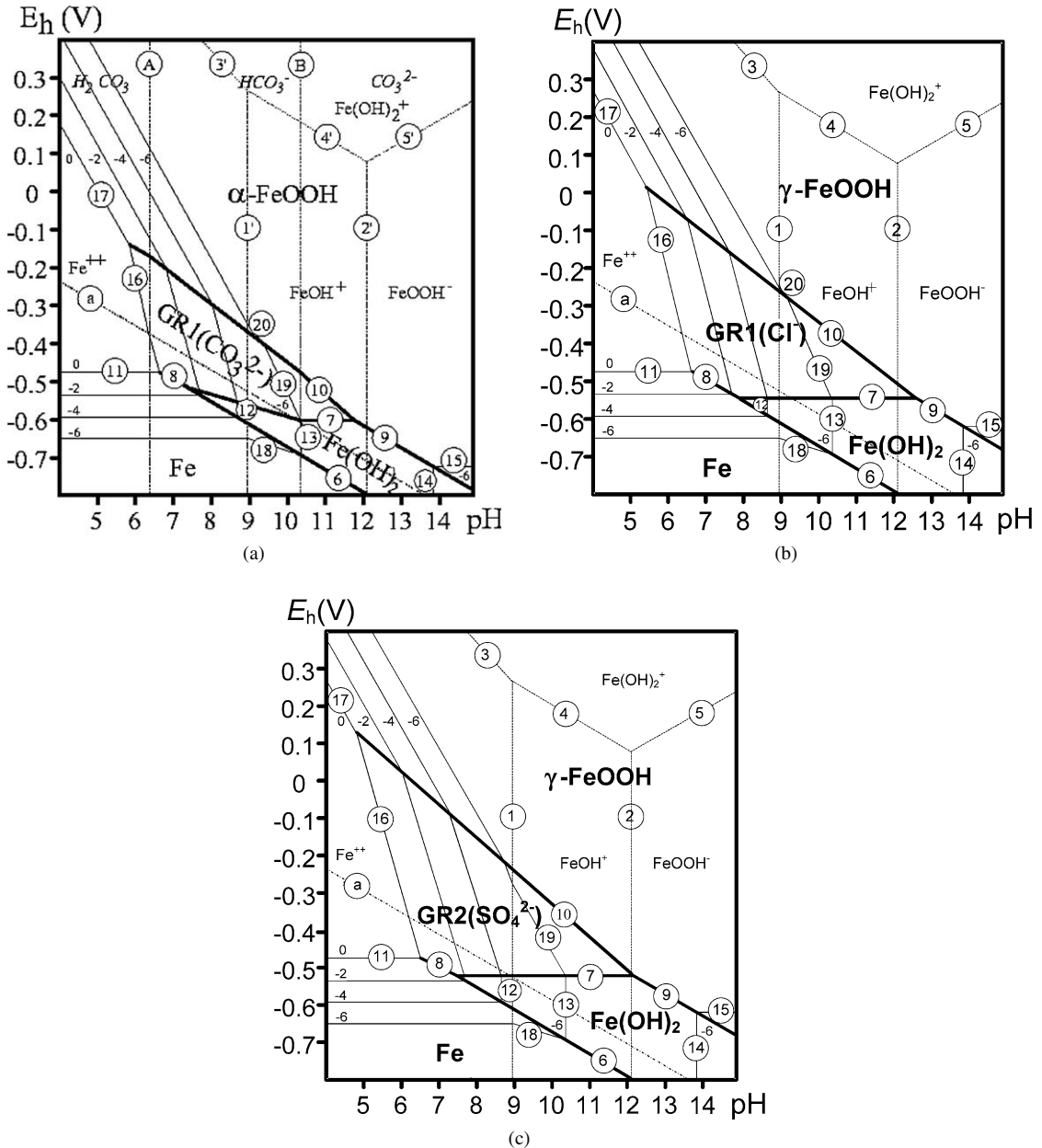


Fig. 10. E_h -pH Pourbaix diagrams for (a) carbonate-, (b) chloride- and (c) sulphate-containing medium where GR1(CO_3^{2-}) [5], GR1(Cl^-) [14] and GR2(SO_4^{2-}) [6] have formulae set at $\text{Fe}_6(\text{OH})_{12}\text{CO}_3$, $\text{Fe}_4(\text{OH})_8\text{Cl}$ and $\text{Fe}_6(\text{OH})_{12}\text{SO}_4$, respectively. The concentrations of anion species are noted ($-n$) meaning 10^{-n} M.

Fig. 10. Diagrammes de Pourbaix E_h -pH pour les milieux contenant (a) des carbonates, (b) des chlorures et (c) des sulfates, où GR1(CO_3^{2-}) [5], GR1(Cl^-) [14] et GR2(SO_4^{2-}) [6] ont des formules établies respectivement à $\text{Fe}_6(\text{OH})_{12}\text{CO}_3$, $\text{Fe}_4(\text{OH})_8\text{Cl}$ et $\text{Fe}_6(\text{OH})_{12}\text{SO}_4$. Les concentrations en espèces anioniques sont désignées par ($-n$), signifiant 10^{-n} M.

supplanted it [2,22,23]. However, one major advantage of disposing of the E_h and pH vs. time curves is that equilibrium data for various concentrations of the solution allowed us to obtain the E_h -pH diagrams. Fig. 10 displays the Pourbaix diagrams of the 3 ma-

jor GRs, i.e. GR1(CO_3^{2-}) [5], GR1(Cl^-) [14] and GR2(SO_4^{2-}) [6] from data collected over the years. Water molecules have been suppressed and formulae are set at $\text{Fe}_6(\text{OH})_{12}\text{CO}_3$, $\text{Fe}_4(\text{OH})_8\text{Cl}$ and $\text{Fe}_6(\text{OH})_{12}\text{SO}_4$. Table 1 gathers the equations of the various reactions

Table 1

Equilibrium equations of E_h -pH Pourbaix diagram reactions for various green rusts: GR1(CO_3^{2-}) [5], GR1(Cl^-) [14] and GR2(SO_4^{2-}) [6]. Formulae are established without water molecules as: $\text{Fe}_6(\text{OH})_{12}\text{CO}_3$, $\text{Fe}_4(\text{OH})_8\text{Cl}^{\text{a}}$, $\text{Fe}_6(\text{OH})_{12}\text{SO}_4$, respectively (cf. Fig. 9).

Tableau 1

Équations d'équilibre des réactions de diagrammes de Pourbaix E_h -pH pour diverses rouilles vertes : GR1(CO_3^{2-}) [5], GR1(Cl^-) [14] et GR2(SO_4^{2-}) [6]. Les formules sont établies sans molécules d'eau, comme étant respectivement : $\text{Fe}_6(\text{OH})_{12}\text{CO}_3$, $\text{Fe}_4(\text{OH})_8\text{Cl}^{\text{a}}$, $\text{Fe}_6(\text{OH})_{12}\text{SO}_4$ (cf. Fig. 9)

<i>Water/Eau</i>	
(a)	$\text{H}_2 \rightleftharpoons 2\text{H}^+ + 2\text{e}^- E_h$ $E_h = 0.000 - 0.0591 \text{ pH}$
<i>Carbonate species/Espèces carbonatées</i>	
(A)	$\text{H}_2\text{CO}_3 \rightleftharpoons \text{HCO}_3^- + \text{H}^+$ $6.37 = \log[\text{H}_2\text{CO}_3] - \log[\text{HCO}_3^-] + \text{pH}$
(B)	$\text{HCO}_3^- \rightleftharpoons \text{CO}_3^{2-} + \text{H}^-$ $10.34 = \log[\text{HCO}_3^-] - \log[\text{CO}_3^{2-}] + \text{pH}$
<i>Iron species/Espèces du fer</i>	
(1)	$\text{Fe}^{2+} + \text{H}_2\text{O} \rightleftharpoons \text{FeOH}^+ + \text{H}^+$ $8.98 = \log[\text{Fe}^{2+}] - \log[\text{FeOH}^+] + \text{pH}$
(2)	$\text{FeOH}^+ + \text{H}_2\text{O} \rightleftharpoons \text{FeOOH}^- + 2\text{H}^+$ $12.10 = 0.5 \log[\text{FeOH}^+] - 0.5 \log[\text{FeOOH}^-] + \text{pH}$
(3)	$\text{Fe}^{2+} + 2\text{H}_2\text{O} \rightleftharpoons \text{Fe}(\text{OH})_2 + 2\text{H}^+ + \text{e}^-$ $E_h = 1.324 - 0.0591 \log[\text{Fe}^{2+}] + 0.0591 \log[\text{Fe}(\text{OH})_2^+] - 0.1182 \text{ pH}$
(4)	$\text{FeOH}^+ + \text{H}_2\text{O} \rightleftharpoons \text{Fe}(\text{OH})_2^+ + \text{H}^+ + \text{e}^-$ $E_h = 0.79 - 0.0591 \log[\text{FeOH}^+] + 0.0591 \log[\text{Fe}(\text{OH})_2^+] - 0.0591 \text{ pH}$
(5)	$\text{FeOOH}^- + \text{H}^+ \rightleftharpoons \text{Fe}(\text{OH})_2^+ + \text{e}^-$ $E_h = -0.638 - 0.0591 \log[\text{FeOOH}^-] + 0.0591 \text{ pH} + 0.0591 \log[\text{Fe}(\text{OH})_2^+]$
(6)	$\text{Fe} + 2\text{H}_2\text{O} \rightleftharpoons \text{Fe}(\text{OH})_2 + 2\text{H}^+ + 2\text{e}^-$ $E_h = -0.080 - 0.0591 \text{ pH}$
(7)	Carbonate-containing medium/Milieu contenant des carbonates
(a)	$6\text{Fe}(\text{OH})_2 + \text{CO}_3^{2-} \rightleftharpoons \text{Fe}_6(\text{OH})_{12}\text{CO}_3 + 2\text{e}^-$ $E_h = -0.63 - 0.0296 \log[\text{CO}_3^{2-}]$
(b)	$6\text{Fe}(\text{OH})_2 + \text{HCO}_3^- \rightleftharpoons \text{Fe}_6(\text{OH})_{12}\text{CO}_3 + \text{H}^+ + 2\text{e}^-$ $E_h = -0.33 - 0.0296 \log[\text{HCO}_3^-] - 0.0296 \text{ pH}$
(7)	Chloride-containing medium/Milieu contenant des chlorures
	$4\text{Fe}(\text{OH})_2 + \text{Cl}^- \rightleftharpoons \text{Fe}_4(\text{OH})_8\text{Cl} + \text{e}^-$ $E_h = -0.57 - 0.0591 \log[\text{Cl}^-]$
(7)	Sulphate-containing medium/Milieu contenant des sulfates
	$6\text{Fe}(\text{OH})_2 + \text{SO}_4^{2-} \rightleftharpoons \text{Fe}_6(\text{OH})_{12}\text{SO}_4 + 2\text{e}^-$ $E_h = -0.55 - 0.0296 \log[\text{SO}_4^{2-}]$
(8)	Carbonate-containing medium/Milieu contenant des carbonates
	$6\text{Fe} + \text{HCO}_3^- + 12\text{H}_2\text{O} \rightleftharpoons \text{Fe}_6(\text{OH})_{12}\text{CO}_3 + 13\text{H}^+ + 14\text{e}^-$ $E_h = -0.12 - 0.0042 \log[\text{HCO}_3^-] - 0.0549 \text{ pH}$
(8)	Chloride-containing medium/Milieu contenant des chlorures
	$4\text{Fe} + \text{Cl}^- + 8\text{H}_2\text{O} \rightleftharpoons \text{Fe}_4(\text{OH})_8\text{Cl} + 8\text{H}^+ + 9\text{e}^-$ $E_h = -0.13 - 0.0066 \log[\text{Cl}^-] - 0.0525 \text{ pH}$
(8)	Sulphate-containing medium/Milieu contenant des sulfates
	$6\text{Fe} + \text{SO}_4^{2-} + 12\text{H}_2\text{O} \rightleftharpoons \text{Fe}_6(\text{OH})_{12}\text{SO}_4 + 12\text{H}^+ + 14\text{e}^-$ $E_h = -0.15 - 0.0042 \log[\text{SO}_4^{2-}] - 0.0507 \text{ pH}$
(9)	$\text{Fe}(\text{OH})_2 \rightleftharpoons \text{FeOOH} + \text{H}^+ + \text{e}^-$ $E_h = E^\circ - 0.0591 \text{ pH}, \text{ with } E^\circ = 0.097 \text{ and } 0.197 \text{ V for } \alpha\text{- and } \gamma\text{-FeOOH, respectively}$
(10)	Carbonate-containing medium/Milieu contenant des carbonates
(a)	$\text{Fe}_6(\text{OH})_{12}\text{CO}_3 \rightleftharpoons 6\alpha - \text{FeOOH} + \text{CO}_3^{2-} + 6\text{H}^+ + 4\text{e}^-$ $E_h = 0.46 + 0.0148 \log[\text{CO}_3^{2-}] - 0.0887 \text{ pH}$
(b)	$\text{Fe}_6(\text{OH})_{12}\text{CO}_3 \rightleftharpoons 6\alpha\text{-FeOOH} + \text{HCO}_3^- + 5\text{H}^+ + 4\text{e}^-$ $E_h = 0.31 + 0.0148 \log[\text{HCO}_3^-] - 0.0739 \text{ pH}$
(c)	$\text{Fe}_6(\text{OH})_{12}\text{CO}_3 \rightleftharpoons 6\alpha\text{-FeOOH} + \text{H}_2\text{CO}_3 + 4\text{H}^+ + 4\text{e}^-$ $E_h = 0.215 + 0.0148 \log[\text{H}_2\text{CO}_3] - 0.0591 \text{ pH}$

Table 1 (continued)

(10) Chloride-containing medium/Milieu contenant des chlorures	$\text{Fe}_4(\text{OH})_8\text{Cl} \rightleftharpoons 4\gamma\text{-FeOOH} + \text{Cl}^- + 4\text{H}^+ + 3\text{e}^-$
	$E_h = 0.45 + 0.0197 \log[\text{Cl}^-] - 0.0788 \text{ pH}$
(10) Sulphate-containing medium/Milieu contenant des sulfates	$\text{Fe}_6(\text{OH})_{12}\text{SO}_4 \rightleftharpoons 6\gamma\text{-FeOOH} + \text{SO}_4^{2-} + 6\text{H}^+ + 4\text{e}^-$
	$E_h = 0.57 + 0.0148 \log[\text{SO}_4^{2-}] - 0.0887 \text{ pH}$
(11) $\text{Fe} \rightleftharpoons \text{Fe}^{2+} + 2\text{e}^-$	$E_h = -0.474 + 0.0296 \log[\text{Fe}^{2+}]$
(12) $\text{Fe}^{2+} + 2\text{H}_2\text{O} \rightleftharpoons \text{Fe}(\text{OH})_2 + 2\text{H}^+$	$13.33 = \log[\text{Fe}^{2+}] + 2 \text{ pH}$
(13) $\text{FeOH}^+ + \text{H}_2\text{O} \rightleftharpoons \text{Fe}(\text{OH})_2 + \text{H}^+$	$4.35 = \log[\text{FeOH}^+] + \text{pH}$
(14) $\text{Fe}(\text{OH})_2 \rightleftharpoons \text{FeOOH}^- + \text{H}^+$	$19.85 = -\log[\text{FeOOH}^-] + \text{pH}$
(15) $\text{FeOOH}^- \rightleftharpoons \text{FeOOH} + \text{e}^-$	$E_h = E^\circ - 0.0591 \log[\text{FeOOH}^-]$, with $E^\circ = -1.08$ and -0.98 V for α - and γ -FeOOH, respectively.
(16) Carbonate-containing medium/Milieu contenant des carbonates	
(a) $6\text{Fe}^{2+} + \text{HCO}_3^- + 12\text{H}_2\text{O} \rightleftharpoons \text{Fe}_6(\text{OH})_{12}\text{CO}_3 + 13\text{H}^+ + 2\text{e}^-$	
	$E_h = 2.04 - 0.1773 \log[\text{Fe}^{2+}] - 0.0296 \log[\text{HCO}_3^-] - 0.3842 \text{ pH}$
(b) $6\text{Fe}^{2+} + \text{H}_2\text{CO}_3 + 12\text{H}_2\text{O} \rightleftharpoons \text{Fe}_6(\text{OH})_{12}\text{CO}_3 + 14\text{H}^+ + 2\text{e}^-$	
	$E_h = 2.23 - 0.1773 \log[\text{Fe}^{2+}] - 0.0296 \log[\text{H}_2\text{CO}_3] - 0.4137 \text{ pH}$
(16) Chloride-containing medium/Milieu contenant des chlorures	
$4\text{Fe}^{2+} + \text{Cl}^- + 8\text{H}_2\text{O} \rightleftharpoons \text{Fe}_4(\text{OH})_8\text{Cl} + 8\text{H}^+ + \text{e}^-$	
	$E_h = 2.58 - 0.2364 \log[\text{Fe}^{2+}] - 0.0591 \log[\text{Cl}^-] - 0.4728 \text{ pH}$
(16) Sulphate-containing medium/Milieu contenant des sulfates	
$6\text{Fe}^{2+} + \text{SO}_4^{2-} + 12\text{H}_2\text{O} \rightleftharpoons \text{Fe}_6(\text{OH})_{12}\text{SO}_4 + 12\text{H}^+ + 2\text{e}^-$	
	$E_h = 1.82 - 0.1773 \log[\text{Fe}^{2+}] - 0.0296 \log[\text{SO}_4^{2-}] - 0.3546 \text{ pH}$
(17) $\text{Fe}^{2+} + 2\text{H}_2\text{O} \rightleftharpoons \text{FeOOH} + 3\text{H}^+ + \text{e}^-$	
	$E_h = E^\circ - 0.0591 \log[\text{Fe}^{2+}] - 0.1773 \text{ pH}$, with $E^\circ = 0.89$ and 0.99 V for α - and γ -FeOOH, respectively.
(18) $\text{Fe} + \text{H}_2\text{O} \rightleftharpoons \text{FeOH}^+ + \text{H}^+ + 2\text{e}^-$	
	$E_h = -0.21 + 0.0296 \log[\text{FeOH}^+] - 0.0296 \text{ pH}$
(19) Carbonate-containing medium/Milieu contenant des carbonates	
$6\text{FeOH}^+ + \text{HCO}_3^- + 6\text{H}_2\text{O} \rightleftharpoons \text{Fe}_6(\text{OH})_{12}\text{CO}_3 + 7\text{H}^+ + 2\text{e}^-$	
	$E_h = 0.45 - 0.1773 \log[\text{FeOH}^+] - 0.0296 \log[\text{HCO}_3^-] - 0.2068 \text{ pH}$
(19) Chloride-containing medium/Milieu contenant des chlorures	
$4\text{FeOH}^+ + \text{Cl}^- + 4\text{H}_2\text{O} \rightleftharpoons \text{Fe}_4(\text{OH})_8\text{Cl} + 4\text{H}^+ + \text{e}^-$	
	$E_h = 0.46 - 0.2364 \log[\text{FeOH}^+] - 0.0591 \log[\text{Cl}^-] - 0.2364 \text{ pH}$
(19) Sulphate-containing medium/Milieu contenant des sulfates	
$6\text{FeOH}^+ + \text{SO}_4^{2-} + 6\text{H}_2\text{O} \rightleftharpoons \text{Fe}_6(\text{OH})_{12}\text{SO}_4 + 6\text{H}^+ + 2\text{e}^-$	
	$E_h = 0.23 - 0.1773 \log[\text{FeOH}^+] - 0.0296 \log[\text{SO}_4^{2-}] - 0.1773 \text{ pH}$
(20) $\text{FeOH}^+ + \text{H}_2\text{O} \rightleftharpoons \text{FeOOH} + 2\text{H}^+ + \text{e}^-$	
	$E_h = E^\circ - 0.0591 \log[\text{FeOH}^+] - 0.1182 \text{ pH}$, with $E^\circ = 0.35$ and 0.45 V for α - and γ -FeOOH, respectively.

^a The formula of GR1(Cl⁻) experimentally obtained is often at $x = 0.25$ even though 0.33 can be reached after long aging [13,14]/La formule de GR1(Cl⁻) obtenue expérimentalement est souvent à $x = 0.25$, même si 0,33 peut être atteint après vieillissement prolongé [13,14].

in the Pourbaix diagram, which are extensively used in corrosion studies but also for predicting thermodynamic possibilities to reduce other species in natural environments [7].

6. Conclusion

The aerial oxidation of Fe(OH)₂ in the presence of anions, e.g., Cl⁻, SO₄²⁻ or CO₃²⁻ depends strongly on the initial value of $R = \{\text{OH}^-\}/[\text{Fe}_{\text{total}}]\}$. At sto-

chiometry of Fe(OH)₂, i.e. at $R_h = 2$, only two plateaus are observed whatever the anions and pH starts around 9 to drop down to about 4–5; the final product is magnetite, which hardly evolves to maghemite. In contrast, with an excess of Fe^{II} and typically for $R_g = (5/3) = 1.67$, three plateaus A, B and C are observed, each corresponding to a reaction equilibrium: in A, between Fe(OH)₂, Fe²⁺_{aq} and GR(Aⁿ⁻), in B, between GR(Aⁿ⁻), Fe²⁺_{aq} and FeOOH, and in C, between Fe²⁺_{aq}, FeOOH and Fe³⁺_{aq}, e.g., for SO₄²⁻,

or Fe^{2+}aq , FeOOH , e.g., for CO_3^{2-} , depending on the pH of the solution due to the dissolved anion. GRs appear in circumneutral conditions (Fig. 10) thus playing a major role in the corrosion of steels and natural environments. The ratio $x = \{\text{[Fe}^{\text{III}}\}/\text{[Fe}_{\text{total}}\}\}$ cannot exceed 1/3 for an ordered structure and x belongs to [0.25, 0.33]. The general formula of GRs is $\{\text{Fe}^{\text{II}}_{(2/3+y)}\text{Fe}^{\text{III}}_{(1/3-y)}(\text{OH})_2\}^{(1/3-y)+} \cdot \{(1/3 - y)/n\} \text{A}^n \cdot (m/n)\text{H}_2\text{O}\}^{(1/3-y)-}$, with $0 \leq y < \sim 1/12$.

Other ways of oxidation, e.g., fast oxidation by H_2O_2 , dry oxidation or voltammetry give rise to a deprotonation of the GR in situ, which can be complete, giving the ‘ferric GR’ that keeps essentially the initial structure. Biotic reduction of ferric oxyhydroxides by DIRB leads also to partially deprotoinated GR1(CO_3^{2-})^{*} but the range is limited to $x \in [1/3, 2/3]$ due to a competition with magnetite. It is $[\text{Fe}^{\text{II}}_{6(1-x)}\text{Fe}^{\text{III}}_{6x}\text{O}_{12}\text{H}_{2(7-3x)}]^{2+} \cdot [\text{CO}_3^{2-} \sim 3\text{H}_2\text{O}]^{2-}$, which renders the foogerite mineral isomorphous with pyroaurite and hydrotalcite, belonging to the $R\bar{3}m$ space group.

References

- [1] O. Benali, M. Abdelmoula, P. Refait, J.-M.R. Génin, Effect of orthophosphate on the oxidation products of Fe(II)–Fe(III) hydroxycarbonate: the transformation of green rust to ferrihydrite, *Geochim. Cosmochim. Acta* 65 (2001) 1715–1726.
- [2] J.D. Bernal, D.R. Dasgupta, A.L. Mackay, The oxides and hydroxides of iron and their structural interrelations, *Clay Miner. Bull.* 4 (1959) 15–30.
- [3] F. Bocher, A. Géhin, C. Ruby, J. Ghanbaja, M. Abdelmoula, J.-M.R. Génin, Coprecipitation of Fe(II)–Fe(III) hydroxycarbonate green rust stabilised by phosphate adsorption, *Solid-State Sci.* 6 (2004) 117–124.
- [4] F.V. Chukhrov, B.B. Zvyagin, A.I. Gorshkov, L.P. Ermilova, V.V. Korovushkin, Y.E. Rudnitskaya, N.Y. Yakubovskaya, Ferroxyhyte, a new modification of FeOOH , *Int. Geol. Rev.* 19 (1977) 873–890.
- [5] S.H. Drissi, P. Refait, M. Abdelmoula, J.-M.R. Génin, The preparation and thermodynamic properties of Fe(II)–Fe(III) hydroxide-carbonate (green rust 1); Pourbaix diagram of iron in carbonate-containing aqueous media, *Corros. Sci.* 37 (1995) 2025–2041.
- [6] J.-M.R. Génin, A.A. Olowe, P. Refait, L. Simon, On the stoichiometry and Pourbaix diagram of Fe(II)–Fe(III) hydroxysulfate or sulfate-containing green rust 2: An electrochemical and Mössbauer spectroscopy study, *Corros. Sci.* 38 (1996) 1751–1762.
- [7] J.-M.R. Génin, P. Refait, G. Bourrié, M. Abdelmoula, F. Trolard, Structure and stability of the Fe(II)–Fe(III) green rust ‘foogerite’ mineral and its potential for reducing pollutants in soil solutions, *Appl. Geochem.* 16 (2001) 559–570.
- [8] J.-M.R. Génin, A. Rabha, A. Géhin, M. Abdelmoula, O. Benali, V. Ernstsen, G. Ona-Nguema, C. Upadhyay, C. Ruby, Foogerite and $\text{Fe}^{\text{II}}\text{--}\text{Fe}^{\text{III}}$ hydroxycarbonate green rust; ordering, deprotoination and/or cation substitution; structure of hydrotalcite-like compounds and mythic ferroso hydroxide $\text{Fe(OH)}_{(2+x)}$, *Solid-State Sci.* 7 (2005) 545–572.
- [9] J.-M.R. Génin, M. Abdelmoula, C. Ruby, C. Upadhyay, Speciation of iron; characterisation and structure of green rusts and $\text{Fe}^{\text{II}}\text{--}\text{Fe}^{\text{III}}$ hydroxycarbonate foogerite, *C. R. Geoscience* 338 (2006).
- [10] A. Girard, G. Chaudron, De la constitution des rouilles, *C. R. Acad. Sci. Paris* 200 (1935) 127–130.
- [11] L. Legrand, M. Abdelmoula, A. Géhin, A. Chaussé, J.-M.R. Génin, Electrochemical formation of a new Fe(II)–Fe(III) hydroxy-carbonate green rust: characterisation and morphology, *Electrochim. Acta* 46 (2001) 1815–1822.
- [12] G. Ona-Nguema, M. Abdelmoula, F. Jorand, O. Benali, A. Géhin, J.-C. Block, J.-M.R. Génin, Iron(II, III) hydroxycarbonate green rust formation and stabilization from lepidocrocite bioreduction, *Environ. Sci. Technol.* 36 (2002) 16–20.
- [13] O. Perales Perez, Y. Umetsu, ORP-monitored magnetite formation from aqueous solutions at low temperatures, *Hydrometallurgy* 55 (2000) 35–56.
- [14] P. Refait, J.-M.R. Génin, The oxidation of ferrous hydroxide in chloride-containing aqueous media and Pourbaix diagrams of green rust one, *Corros. Sci.* 34 (1993) 797–819.
- [15] P. Refait, J.-M.R. Génin, The mechanisms of oxidation of ferrous hydroxylchloride $\beta\text{-Fe}_2(\text{OH})_3\text{Cl}$ in aqueous solution: the formation of akaganeite vs. goethite, *Corros. Sci.* 39 (1997) 539–553.
- [16] P. Refait, D. Rézel, J.-M.R. Génin, The corrosion products of iron specific of chloride-containing aqueous media, in: *Progress in the Understanding and Prevention of Corrosion*, The Institute of Materials, London, 1993, pp. 1122–1128.
- [17] P. Refait, A. Charton, J.-M.R. Génin, Identification, composition, thermodynamic and structural properties of a pyroaurite-like iron(II)–iron(III) hydroxy-oxalate green rust, *Eur. J. Solid-State Inorg. Chem.* 35 (1998) 655–666.
- [18] P. Refait, L. Simon, J.-M.R. Génin, Reduction of SeO_4^{2-} anions and anoxic formation of iron(II)–iron(III) hydroxy-selenate green rust, *Environ. Sci. Technol.* 34 (2000) 819–825.
- [19] P. Refait, O. Benali, M. Abdelmoula, J.-M.R. Génin, Formation of ‘ferric green rust’ and/or ferrihydrite by fast oxidation of $\text{Fe}^{\text{II}}\text{--}\text{Fe}^{\text{III}}$ hydroxylchloride green rust, *Corros. Sci.* 45 (2003) 2435–2449.
- [20] E. Roden, Analysis of long-term bacterial vs. chemical Fe(III) oxide reduction kinetics, *Geochim. Cosmochim. Acta* 68 (2004) 3205–3216.
- [21] E. Roden, Geochemical and microbiological controls on dissimilatory iron reduction, *C. R. Geoscience* 338 (2006).
- [22] C. Ruby, A. Géhin, M. Abdelmoula, J.-M.R. Génin, J.-P. Jolivet, Coprecipitation of Fe(II) and Fe(III) cations in sulphated aqueous medium and formation of hydroxysulphate green rust, *Solid-State Sci.* 5 (2004) 1055–1062.
- [23] C. Ruby, R. Aissa, A. Géhin, J. Cortot, M. Abdelmoula, Green-rust synthesis by coprecipitation of $\text{Fe}^{\text{II}}\text{--}\text{Fe}^{\text{III}}$ ions and mass-balance diagrams, *C. R. Geoscience* 338 (2006).
- [24] L. Simon, J.-M.R. Génin, P. Refait, Standard free enthalpy of formation of Fe(II)–Fe(III) hydroxysulfite green rust one and its oxidation into hydroxysulfate green rust two, *Corros. Sci.* 39 (1997) 1673–1685.
- [25] J. Vins, J. Subrt, V. Zapletal, F. Hanousek, Preparation and properties of green rust type substances, *Coll. Czech. Chem. Commun.* 52 (1987) 93–102.